International Journal of Applied Power Engineering (IJAPE)
Vol. 15, No. 2, June 2026, pp. 818∼830
ISSN: 2252-8792, DOI: 10.11591/ijape.v15.i2.pp818-830

Wind direction based aggregation of wind power plants under exact wind speeds

Ali M. S. Al-Bayati[1], Huda Hamza Abdulkhudhur[2]
[1]Department of Mathematics, College of Education Tuz Khurmatu, Tikrit University, Tuz Khurmatu, Iraq
[2]Department of Cybersecurity Techniques Engineering, Technical Engineering College for Computer and AI-Kirkuk, Northern Technical University, Kirkuk, Iraq

Article Info

Article history:

Received May 27, 2025
Revised Feb 25, 2026
Accepted Mar 12, 2026

Keywords:

Aggregated models
Wind power plant
Wind power plant aggregation
Wind speed directions
Wind turbine

ABSTRACT

Modeling of a wind power plant (WPP) containing numerous wind turbines in a highly detailed manner requires a substantial computational cost. Further, the response and dynamic behavior of the WPP systems are significantly influenced by the dynamic nature of wind speed. This paper presents a methodology of aggregating WPP systems with consideration for wind speed directions. To attain a realistic aggregated model, an algorithm for calculating actual exact wind speed at each wind turbine within the WPP was proposed considering different wind speed directions. Furthermore, the best wind speed direction for a fixed site area that produces a minimum wind energy losses inside the WPP was also assessed and reported. The results revealed the importance of employing the exact wind speed calculations within the WPP to ensure that the aggregated WPP model accurately represents real-world conditions. The results of this paper highlighted the role of wind direction in determining the response of WPPs and provide guidance on maximizing the WPP throughput during the year under the prevailing wind speed direction at the site.

Corresponding Author:

Ali M. S. Al-Bayati
Department of Mathematics, College of Education Tuz Khurmatu, Tikrit University
Tuz Khurmatu, Salah Al-Din, Iraq
Email: ali.mah.salman@tu.edu.iq

1. INTRODUCTION

Over the past few years, electrical power systems have changed significantly as a result of large penetration of renewable sources of energy. In wind power sector, a considerable number of wind power plants (WPPs) have been combined with the existing power systems across the world. In the third quarter of 2023, about 288 MW of land-based wind power production was incorporated to the USA power system, which increased the cumulative operating land-based wind power to over 146 GW [1]. In Europe, many countries like UK, Germany, and Spain reached to advanced stages of power generation depending on wind energy. In 2022, a 19 GW of new wind power was integrated to the grid in Europe [2]. Significant focus has been directed towards wind power in Asia, where China and India ranked among the top five markets worldwide in terms of cumulative installations at the end of 2021 [3].

The WPP's electric power throughput primarily relies on the value of wind speed that receives by each individual wind turbine where it can be assessed as input fuel to the turbines. These wind speeds also determine the dynamic response of the WPP under load fluctuations and fault conditions at the moment of the event. From this standpoint, it is very important to determine the actual exact wind speeds and use them in

the WPP system's studies. The wind speed distribution within a WPP is not uniform and it is different from one location to another. Therefore, the wind distribution cannot be considered constant at all locations within the WPP. Many research works have been conducted in the literature to develop and investigate different wind speed forecasting models. The result in [4] combined the autoregressive moving average with the support vector regression to form a hybrid approach for modeling and predicting the wind speed. An approximation method of wind speed distribution was proposed with the aim to accurately estimate the WPPs' output generation [5]. Silveira *et al.* [6] used the Normal-Weibull-Weibull as a mixture distribution model for modeling wind speed data, while Zhang *et al.* [7] presented a prediction method for wind speed in the WPP clusters considering the spatial characteristics. Wind speed data were generated at every 1 sec for a given WPP's site to be used in the dynamic studies of power systems integrated with WPPs [8]. While the above-mentioned research efforts provide valuable insight into the modeling and forecasting of wind speeds, they did not test or apply the generated wind speed data to the aggregate models of WPPs.

In aggregate modeling of WPPs, numerous number of wind turbines are represented by one or few equivalent machines. The wind speeds that are received by the equivalent machines have to be appropriately calculated such that the aggregated model accurately represents the entire WPP as closely as possible. In the context of WPP aggregation and wind speeds' calculation, study in [9] assumed a WPP of only one section of wind turbines where the different wind incidents affecting the turbines were disregarded. However, other works were assumed that the wind speed is reduced by a specific amount constant number (5 percent of incoming wind speed, 0.5 m/sec, 1 m/sec) per row or section without calculating the exact wind speeds that receive by the wind turbines within the WPP [10], [11]. An equivalent wind speed model was discussed to be used in the equivalent aggregated model [12]. However, the developed model was not able to reflect both the exact wind losses and the dynamic response of the WPP. Wang *et al.* [13] presented different approaches to aggregate the impedances of the turbines and internal network of a WPP. A comparison study [14], [15] was performed between the predicted and measured output power for a WPP. The wake effect model was taken into consideration to show its influence on the predicted power from a WPP. The studies [16], [17] presented aggregated models that may be used to represent the entire WPP in stability analysis. Four different types of WPPs were used to study and implement the wake effect model in the power systems' simulation [18]. However, neither the aggregated model of the WPPs nor the wind speed that is received by every individual turbine were presented properly. Rahman *et al.* [19] used multiple probabilistic clustering algorithms to study and evaluate the performance of the aggregated WPP. The result in [20] showed the inadequacy of full aggregated model of WPPs due to ignoring the effects of different wind speeds within the WPPs. Shabanikia *et al.* [21] proposed weighted dynamic aggregation method to find an equivalent aggregated model for a WPP incorporating induction generator wind turbines. Han *et al.* [22] used multivariate multi-scale entropy method to aggregate the WPPs. Jin *et al.* [23] proposed a combination model to calculate the wind speeds at the turbines with application to the aggregated model taking into account the wind turbines' low voltage ride through characteristics. Yet, the wind speed relation with the WPP configuration as well as the arrangement of the wind turbines were not considered.

Although many aggregation models of WPPs take into consideration wind direction and spatial effects, this paper contributes by proposing a simple methodological approach for calculating the actual exact speed of wind incident at every wind turbine within the WPPs depending on an incoming real wind speed profile. Towards a realistic aggregated model, a methodology of aggregating WPP systems under different wind speed directions was presented taking into account the calculated actual exact wind speeds. Comparison and analysis were conducted on the performance of WPP to assess the impact of considering or disregarding the actual exact wind speeds. The analysis was performed under different wind speed directions with the aim of identifying the most favorable direction that results in reduced wind energy losses. This work is organized as follows: section 2 introduces methodology for calculating actual exact wind speeds and the WPP aggregation under different wind directions, section 3 presents and discusses the results of the paper, and section 4 outlines the conclusions.

2. METHOD

2.1. Wind speed modeling

Wind speed fluctuations have an enormous influence on the dynamic response of wind turbines. This is owing to a significant cubic relation that relates the speed of wind with the extracted power from the turbine as described by (1).

$$P = 0.5\rho A C_p(\lambda, \beta) V_{\mathrm{W}}^3(t) \quad (1)$$

Where P, ρ, A, C_p, λ, β, and $V_{\mathrm{W}}(t)$ are the turbine mechanical power, air density, blades' sweep area, turbine power coefficient, tip speed ratio, blades' pitch angle, and speed of wind, respectively.

In general, the wind speed modeling relies on four components that comprise together the wind speed. Those are the basic, gust, ramp, and turbulence wind components. The sum of those components gives the wind speed that a turbine receives at any moment and it takes the form of [24].

$$V_{\mathrm{W}}(t) = V_{\mathrm{WB}} + V_{\mathrm{WG}}(t) + V_{\mathrm{WR}}(t) + V_{\mathrm{WN}}(t) \tag{2}$$

Where V_{WB}, V_{WG}, V_{WR}, and V_{WN} are the basic, gust, ramp, and turbulence wind speed components, respectively. The basic wind speed component can be considered constant among the WPP while the gust wind speed component changes as a function of time [24] as it is expressed by (3).

$$V_{\mathrm{WG}}(t) = \begin{cases} 0, & t < T_1 \\ C\left(1 - \cos\left(2\pi \cdot \dfrac{t - T_1}{T_2 - T_1}\right)\right), & T_1 \leq t \leq T_2 \\ 0, & t > T_2 \end{cases} \tag{3}$$

Where C, T_1, and T_2 are a constant that represents a percentage of the gust maximum value in m/sec, the start time of the gust component in sec, and the end time of the gust component in sec, respectively. The ramp wind speed component is also a function of time [24] where it is given by (4).

$$V_{\mathrm{WR}}(t) = \begin{cases} 0, & t < T_3 \\ C_1\left(\pi \cdot \dfrac{t - T_3}{T_4 - T_3}\right), & T_3 \leq t \leq T_4 \\ 0, & t > T_4 \end{cases} \tag{4}$$

Where C_1, T_3, and T_4 are a constant that represents the ramp maximum value in m/sec, the start time of the ramp component in sec, and the end time of the ramp component in sec, respectively. The turbulence (noise) wind component takes the form of (5).

$$V_{\mathrm{WN}}(t) = \sum_{i=1}^{n} \sqrt{S_{\mathrm{WN}}(f_i)\,\Delta f} \cdot \cos\left(2\pi f_i t + \theta_i + \Delta\phi\right) \tag{5}$$

Where $S_{\mathrm{WN}}(f_i)$ is the turbulence (noise) spectral density and it is defined by (6).

$$S_{\mathrm{WN}}(f) = \frac{\frac{l V_{\mathrm{WB}}}{\ln\left(\frac{H}{Z_{\mathrm{o}}}\right)^2}}{\left(1 + \frac{1.5 f l}{V_{\mathrm{WB}}}\right)^{\frac{5}{3}}} \tag{6}$$

Where f_i, θ_i, $\Delta\phi$, l, H, and Z_{o} are the frequency, initial phase, phase component, turbulent length scale, wind hub height in m, and roughness length, respectively. It should be noted that the value of Δf falls between 0.1 Hz and 0.3 Hz while the value of l equals to 20 m for H less than 30 m and it is equal to 600 m for H larger than 30 m [25].

2.2. Algorithm for actual exact wind speeds' calculations within the WPP

In a particular WPP layout, the incoming wind speed received by every single wind turbine in a row or a section will reduce due to shadowing and wind turbulence among the WPP. This phenomenon will continue among the whole WPP between each upstream row (or section) and the next downstream row (or section). The wind speed at every individual turbine within the WPP is obtained by (7) [8].

$$V_{\mathrm{W}}(t, x) = V_{\mathrm{Wo}}(t)\Big(1 - \Big(\frac{R}{K_{\mathrm{w}} x + R}\Big)^2 (1 - \sqrt{1 - C_{\mathrm{t}}})\Big) \tag{7}$$

Where $V_{\mathrm{Wo}}(t)$, R, K_{w}, C_{t}, and $V_{\mathrm{W}}(t, x)$ are the incoming wind speed in m/sec, radius of the turbine rotor in m, wake decay coefficient, thrust coefficient, and the wind speed at any location within the WPP, respectively. It should be noted that the above model is called Jensen's model for wake effect calculation. The wake decay

coefficient is a constant which is defined by experimentally measurements and it ranges from 0.04 to 0.05 for offshore WPP while its value equal to 0.075 for onshore WPP [26]. The C_{t} in (8) is defined as the thrust coefficient [27] and it depends mainly on the receiving wind speed and the turbine type. The thrust coefficient of wind turbine [28] is modeled by (8).

$$C_{\mathrm{t}} = \frac{3.5(2V_{\mathrm{Wo}} - 3.5)}{V_{\mathrm{Wo}}^2} \tag{8}$$

Normally, the wind turbines are distributed and organized on a fixed pattern within the WPP. In most cases, the turbines are divided into rows and columns taking into account the blade length to ensure an appropriate normalized distance (distance/rotor diameter) between the turbines. On the other hand, the overall dimensions of the WPP site, the nature of the ground (smooth or rough lands) as well as the prevailing wind flow direction are important factors that constrain the appropriate wind turbines' positioning within the WPP. It is crucial to distribute the turbines such that they face, to the maximum extent, the possible wind flow in the particular area [8].

A flowchart in Figure 1 illustrates the key steps that were followed in determining the actual exact wind speeds within the WPP. The first step involves defining the WPP layout, specifying the turbines' arrangement inside it, and determining the normalized distance between turbines. After choosing the layout, the wind speed profile that reaches the foremost row (or section) of wind turbines is measured. The wake decay coefficient value is then selected based on the nature of the WPP. To obtain the wind speed at the second row (or section) of wind turbines, the thrust coefficient of the second row's (or section's) of wind turbines is calculated using (8), followed by calculating the wind speed using (7). By using the calculated actual exact wind speed at the second row (or section) as an incoming wind speed, the (7) and (8) are employed to compute the wind speed at the third row (or section) of wind turbines. The process continues with the aim of calculating the actual exact wind speed at every wind turbines' row (or section) within the WPP.

2.3. Aggregation of WPP under different wind directions

In the framework of a model that combines multiple aggregated machines, any row or section of wind turbines among a WPP is capable of being aggregated into a single equivalent machine; thus, the entire WPP is modeled by a multi-machine approach. This model is based actually on the fact of identical operating points for the wind turbines in each row or section as a result of identical received wind speed. The calculated actual exact wind speeds are utilized to aggregate the WPP in Figure 2 employing the multi-machine aggregated approach. It is important to mention that the multi-machine aggregated model is used in this paper among the other aggregated models due to its better ability to capture and provide the WPP's collective response at the connection point with the grid [11]. The effects between ignoring and considering the actual exact wind speeds are shown in terms of WPP's active output power. The weighted mean method was used to aggregate the wind turbines' parameters to get the equivalent parameters of the aggregated model. These equivalent parameters can be computed by (9).

$$\begin{aligned} a_i &= \frac{S_i}{\sum_{i=1}^{n} S_i} \qquad Z_{\mathrm{seq}} = \sum_{i=1}^{n} a_i Z_{\mathrm{s}i} \qquad Z_{\mathrm{req}} = \sum_{i=1}^{n} a_i Z_{\mathrm{r}i} \\ X_{\mathrm{meq}} &= \sum_{i=1}^{n} a_i X_{\mathrm{m}i} \qquad H_{\mathrm{eq}} = \sum_{i=1}^{n} a_i H_i \qquad H_i = H_{\mathrm{t}i} + H_{\mathrm{g}i} \end{aligned} \tag{9}$$

Where a_i is the weight coefficient, $Z_{\mathrm{s}i}$ is the impedance of stator, $Z_{\mathrm{r}i}$ is the impedance of rotor, $X_{\mathrm{m}i}$ is the magnetizing reactance, $H_{\mathrm{t}i}$ is the inertia constant of turbine, and $H_{\mathrm{g}i}$ is the inertia constant of generator [10]. The power ratings of the equivalent generator can be obtained [10] by (10).

$$S_{\mathrm{eq}} = \sum_{i=1}^{n} S_i \qquad\qquad P_{\mathrm{eq}} = \sum_{i=1}^{n} P_i \tag{10}$$

Where S_i and P_i are the apparent and active power ratings of each individual generator while n refers to the generators' number. The aggregation of the internal electrical network of the WPP can be found in [29].

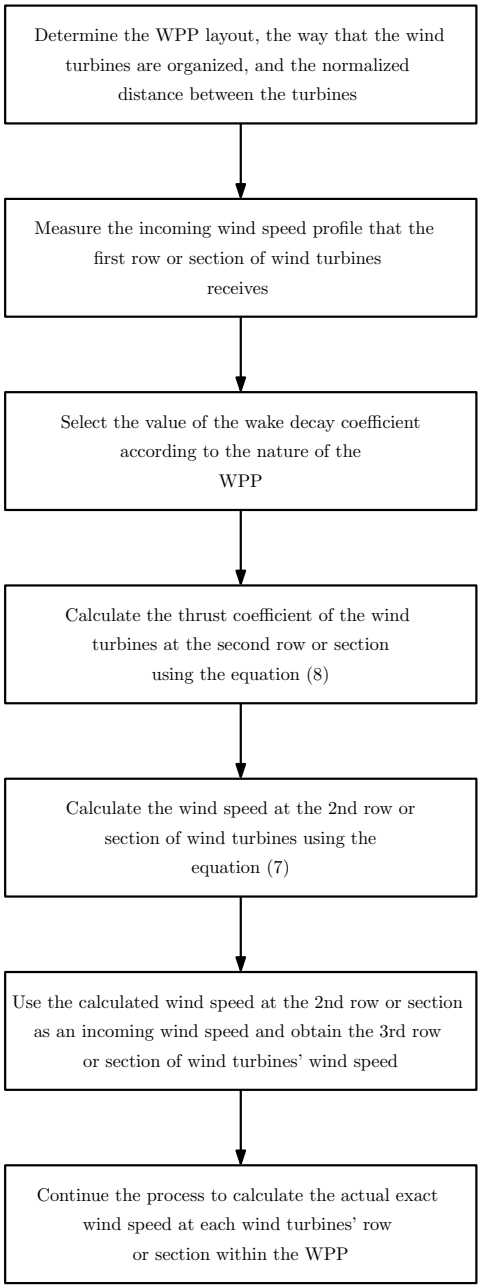

Figure 1. Flowchart diagram showing the steps involved in calculating the actual exact wind speed at every row or section of wind turbines within a WPP

3. RESULTS AND DISCUSSION

The algorithm for calculating the actual exact wind speeds within the WPP as well as the aggregation of wind turbines were performed in MATLAB software. In the WPP under study, there are five sections, each containing four turbines as depicted in Figure 2. The total number of turbines are 20 with 1.5 MW rating each. The type of the generator installed in each wind turbine is a doubly-fed induction generator with 0.00706+j0.171 pu of stator winding impedance (Z_{s}) and 0.005+j0.156 pu of rotor winding impedance (Z_{r}). Each section of wind turbines are connected together at the section busbar through 2 MVA rated transformers and as well as internal transmission lines (Z_i). Further, each section of wind turbines is linked to the station busbar through section transmission line ($Z_{\mathrm{L}i}$) where the entire WPP in turn is connected to the grid via a 47 MVA rated station transformer.

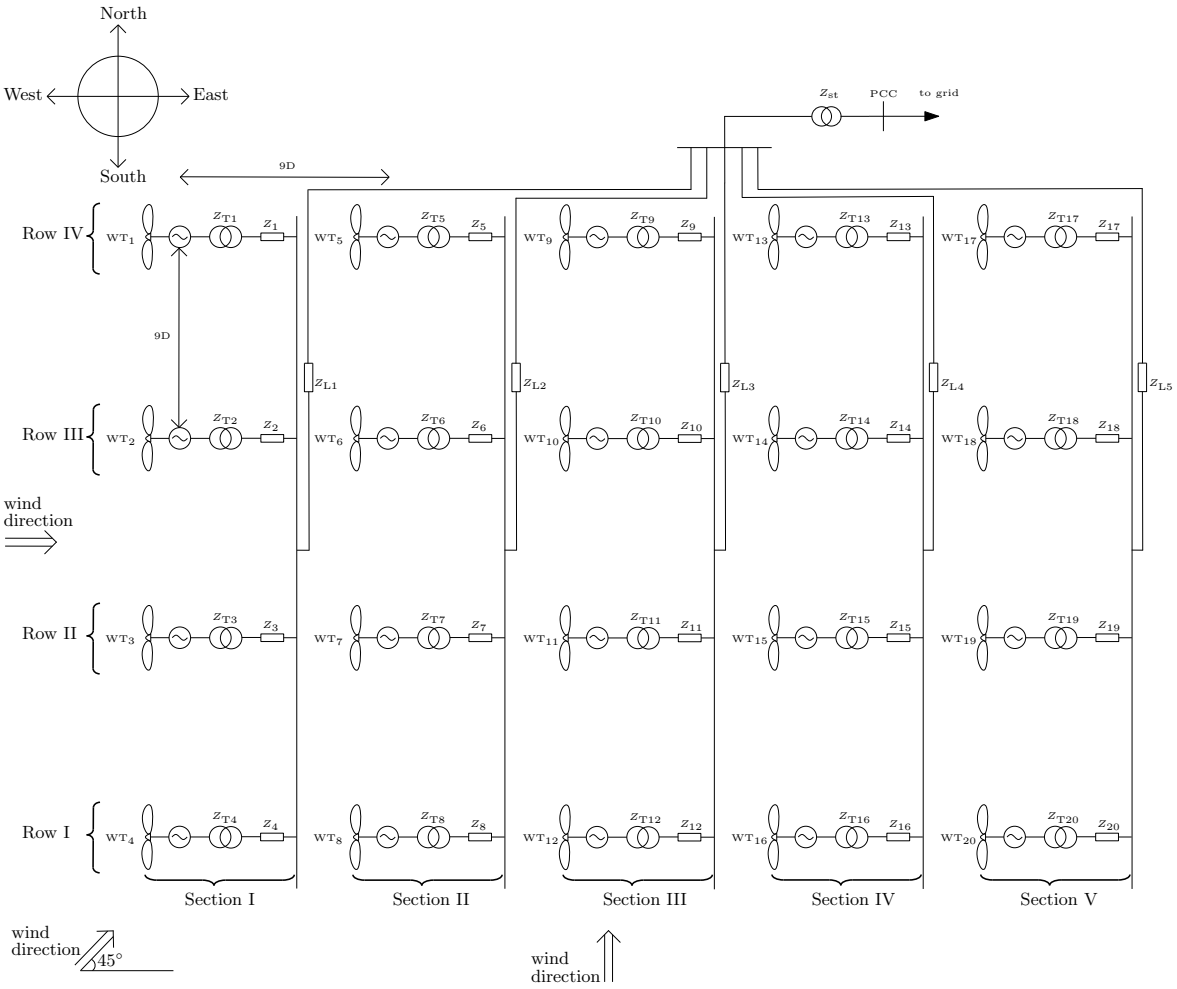

Figure 2. WPP layout under study, where D is the wind turbine blades' diameter

The spacing between the wind turbines within the WPP is normally chosen in away that reduces the overall energy loss due to the wind turbulence. A real wind speed profile was used as an initial incoming wind speed that reaches the first row (or section) of wind turbines inside the WPP. The measurements of the used wind speed profile were gathered in Boulder city, located in the state of Colorado, USA. They were captured with a cup anemometer, measuring at a frequency of 100 Hz, positioned at 36.6 m above ground level. Here, it is worth mentioning that the wind speed at the turbine hub height was computed by utilizing the power-law [30], as given by (11).

$$V_{\mathrm{W_H}} = V_{\mathrm{W_{ane}}} \left(\frac{d_{\mathrm{H}}}{d_{\mathrm{ane}}} \right)^{\alpha} \tag{11}$$

Where $V_{\mathrm{W_H}}$, $V_{\mathrm{W_{ane}}}$, d_{H}, d_{ane}, and α are the wind speed at hub height, wind speed at the anemometer height, turbine hub height, anemometer height, and wind shear exponent, respectively. In this work, the hub height of turbines is 80 m, and the wind shear exponent was assumed to be 0.14 (the typical value for flat terrain) [31].

Three wind speed directions were considered and the actual exact wind speeds were calculated at all the wind turbines within the WPP. It is worth mentioning that each wind direction in Figure 2 is assumed to be fixed and the wind turbines are facing the incoming wind. The actual exact wind speeds' calculations and their importance in aggregating WPP were accomplished and discussed under the following case studies:

3.1. Wind speed direction from west to east

The wind speed were considered to be faced by the wind turbines in the direction from west to east as it is indicated in Figure 2. The spacing among each two consecutive sections of wind turbines was chosen to be nine times the diameter for the turbine blades. The algorithm that was discussed in the previous section was implemented and the actual exact wind speeds at the different sections of wind turbines were calculated as shown in Figure 3. The results show the accurate amount of reduction in the initial incoming wind speed that is faced by the first section of wind turbines as the wind flows among the WPP.

Considering the aforementioned wind speed direction, the entire WPP was aggregated using the multi-machine aggregated model. Figure 4 shows the aggregation of the WPP in Figure 2 under the wind direction west to east. The calculated actual exact wind speeds in Figure 3 were received by the corresponding equivalent wind turbine for each section in the WPP. The WPP's output active power was chosen to show the effect of considering the actual exact wind speeds within the WPP. Figure 5 shows the WPP's output active power under two cases; with 0.5 m/sec decreasing in wind speed at each section (as it is assumed by many works) and with the actual exact wind speed at each wind turbine within the WPP.

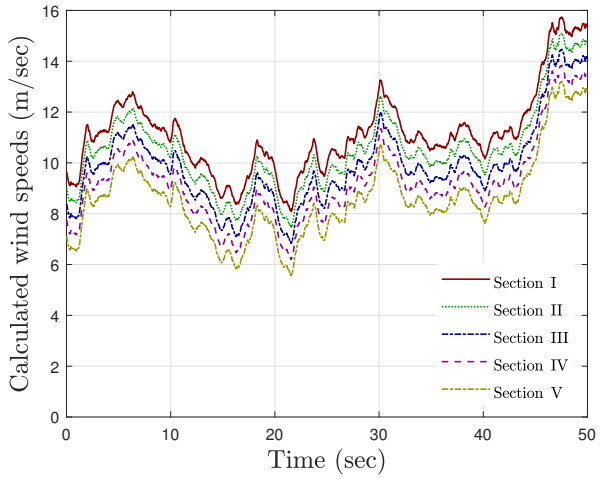

Figure 3. Calculated actual exact wind speeds at different sections of the WPP in Figure 2 under the wind direction west to east

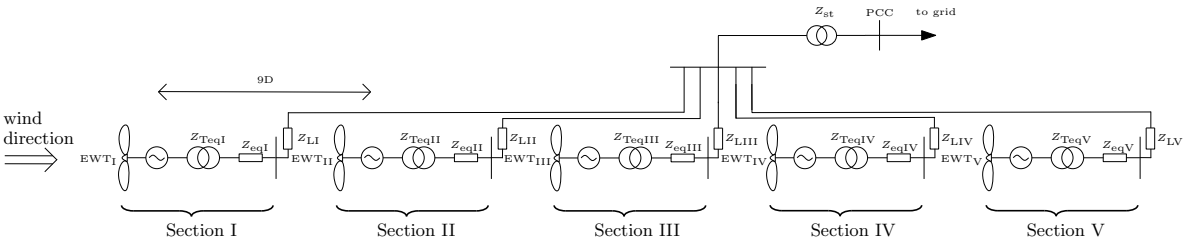

Figure 4. Multi-machine aggregated model under the wind direction west to east

3.2. Wind speed direction from south to north

In this section, it was assumed that the wind speed confronting the turbines flows from the southern direction and proceed in a northerly trajectory as depicted in Figure 2. The WPP under consideration with this wind speed direction comprises four rows with five wind turbines within each row. The initial incoming wind speed that is received by the first row of turbines as well as the distance between each two consecutive rows are the same as in the previous case. The simulation was executed using the same algorithm that was discussed in section 2. The actual exact wind speeds at the different rows within the WPP were calculated and are shown in Figure 6.

The WPP depicted in Figure 2 was aggregated into a multi-machine model under the consideration of south to north wind speed direction. As a result, the whole WPP in Figure 2 is represented as it is given in Figure 7. The calculated actual exact wind speeds, as illustrated in Figure 6, were applied to the corresponding equivalent machines of the WPP. Figure 8 depicts the response of the multi-machine aggregated model under two cases; with 0.5 m/sec decreasing in wind speed at each row and with the actual exact wind speeds received by the wind turbines within the WPP.

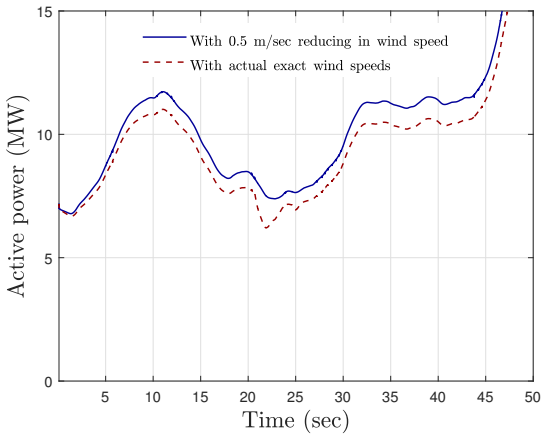

Figure 5. Multi-machine aggregated model response under two cases, with 0.5 m/sec decreasing in wind speed and with the actual exact wind speed at each wind turbine under the wind direction west to east

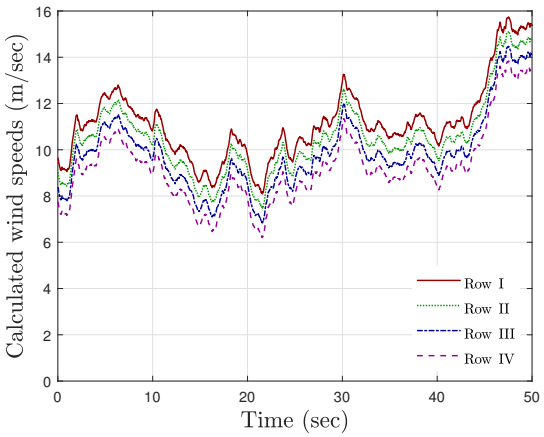

Figure 6. Calculated actual exact wind speeds at different rows of the WPP in Figure 2 under the wind direction south to north

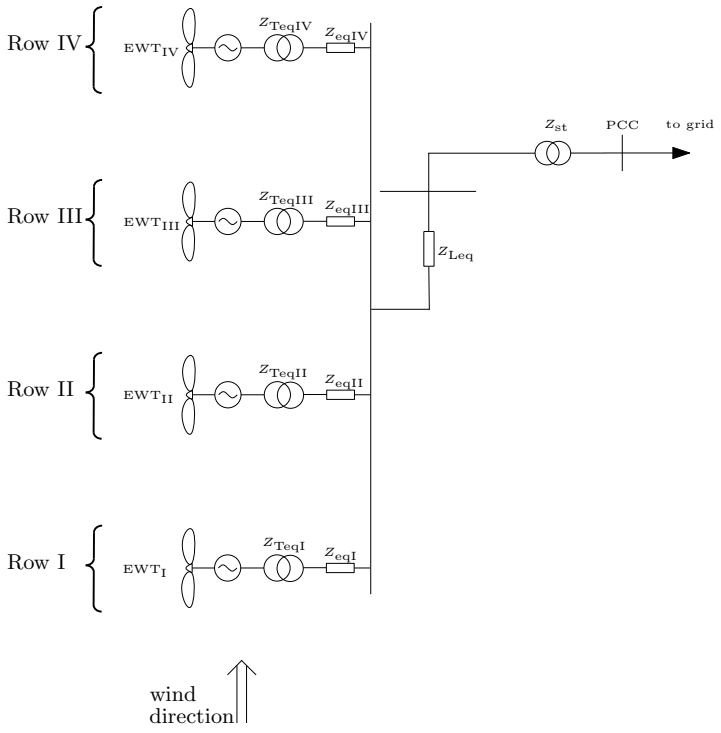

Figure 7. Multi-machine aggregated model under the wind direction south to north

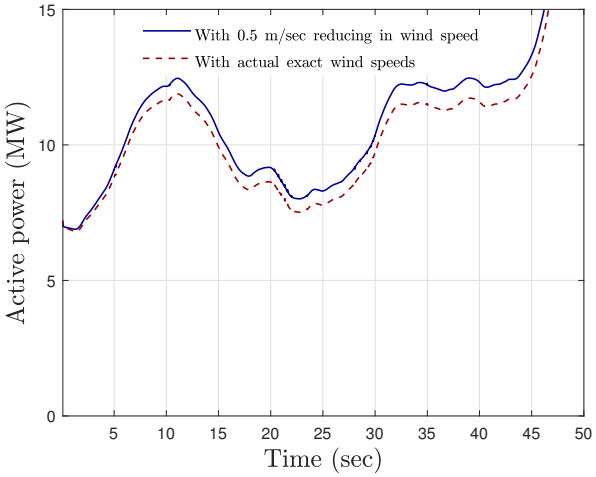

Figure 8. Multi-machine aggregated model response under two cases, with 0.5 m/sec decreasing in wind speed and with the actual exact wind speed at each wind turbine under the wind direction south to north

3.3. Wind speed direction with 45°

The wind speed was considered to flow and face by the wind turbines with 45° as it is depicted in Figure 2. Here, the WPP under study consists of four stages, each comprising a different number of wind turbines. The number of turbines that receive an identical wind speed in each stage can be obtained by (12).

$$ns(i) = N_{\mathrm{S}} + N_{\mathrm{R}} + 1 - 2i \tag{12}$$

Where $i = 1, 2, 3, ...$ is an index that represents the number of stages, N_{S} is the number of sections, N_{R} is the number of rows, and $ns(i)$ represents the total count of turbines in each stage within the WPP. As a result, in stages I, II, III, and IV, there are eight, six, four, and two wind turbines, respectively, that receive an identical wind speed. The distance between the wind turbines of two consecutive stages is $\sqrt{2}(9\mathrm{D})$ where D is the diameter of the turbine blades.

With the specified wind speed direction in consideration, the initial incoming wind speed is directed towards the primary stage, encompassing eight wind turbines. Furthermore, it was adhered to the algorithm outlined in section 2, resulting in the calculation of actual exact wind speeds at distinct stages, as visually represented in Figure 9. Taking into account a wind direction of 45°, the WPP depicted in Figure 2 was aggregated into four equivalent machines. Figure 10 illustrates the WPP aggregated model under wind direction with 45°. The quantity of turbines that was aggregated together in stages I, II, III, and IV are eight, six, four, and two wind turbines, respectively. The same procedure elucidated in the preceding two sections was applied to analyze the response of the aggregated model. The actual exact wind speed that face by each wind turbine within the WPP was used in the simulation. The WPP's active power was used to show the effect of the calculated actual exact wind speeds. Figure 11 shows the WPP's output active power under two scenarios; one with a decrease of 0.5 m/sec in wind speed at each stage and the other with the actual exact wind speeds.

3.4. Assessing WPP throughput across multiple wind speed directions

The dynamic nature of wind speed is a pivotal factor that leads to the variability in WPP power generation. The continual fluctuations and non-constant direction of wind speed increase the challenges and complexity of harnessing wind energy for sustainable power generation. It is paramount of importance to consider actual wind speed profile and different wind directions in evaluating the reliability and throughput of WPPs. This will help to optimally deploy the dynamic nature of wind speed inside WPPs.

Through the presented analysis in the previous sections, it can be seen that there is a contrast between the response of the WPP under the calculated actual exact wind speeds and the assumption of a 0.5 m/sec reduction commonly used in the literature. This contrast highlights the importance of accounting for actual exact wind speeds within the WPP in aggregating large wind farms. The actual response of an aggregated model of a WPP will be more realistic and beneficial in studying the dynamic response of power systems when

integrated with large WPPs. The obtained results reveal that the highest output power of the WPP attained under the wind direction of 45° as shown in Figure 12. This observation emphasizes the significance of wind speed direction in maximizing the throughput of WPPs. Therefore, a precise understanding of wind patterns in a specific geographic region is critical for the effective placement of the turbines within a WPP. The WPPs have to be constructed such that the quantity of wind turbines receiving an identical level of wind speed is maximized on one hand, and the wind energy loss is minimized on the other hand.

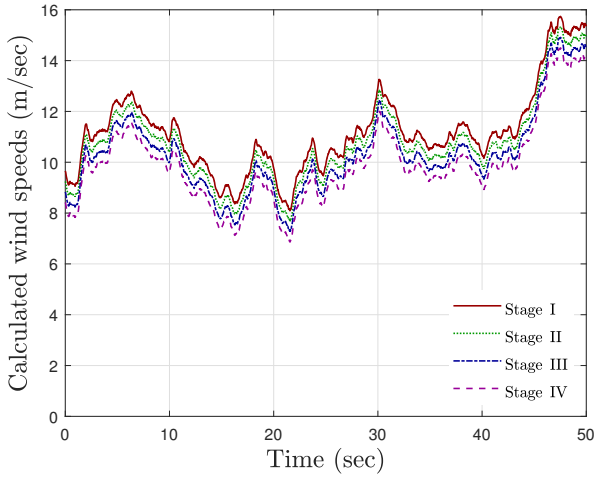

Figure 9. Calculated actual exact wind speeds at different stages of the WPP in Figure 2 under the wind direction with 45°

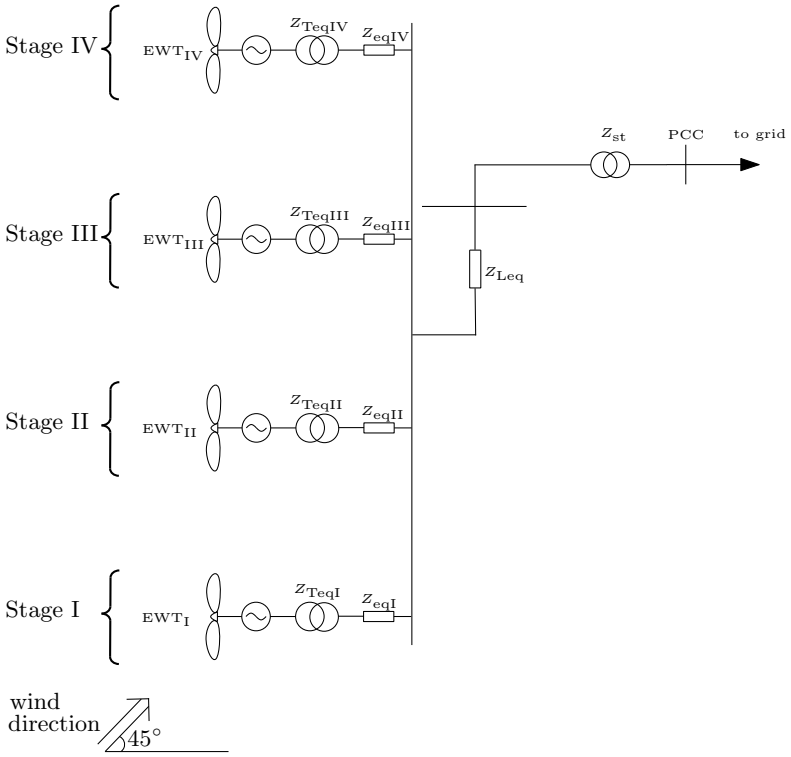

Figure 10. Multi-machine aggregated model under wind direction with 45°

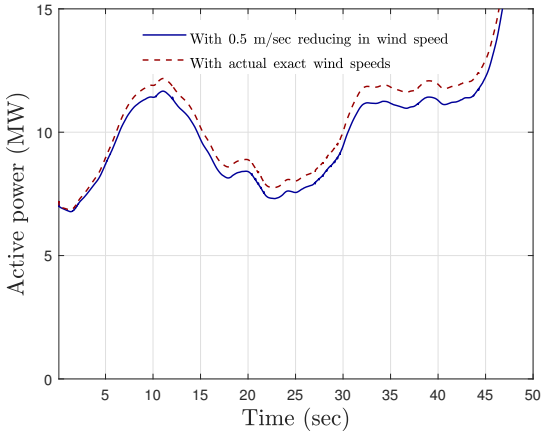

Figure 11. Multi-machine aggregated model response under two cases, with 0.5 m/sec decreasing in wind speed and with the actual exact wind speed at each wind turbine with 45° wind direction

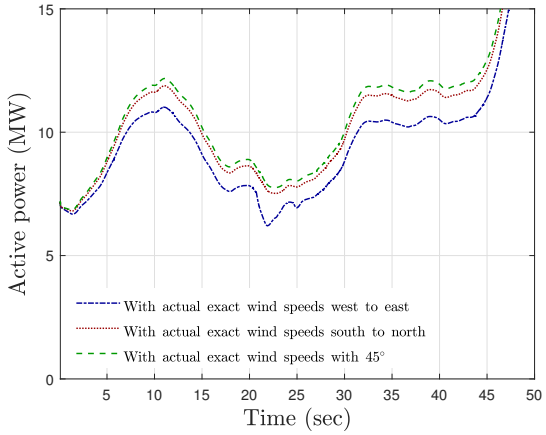

Figure 12. Throughput of the WPP under different wind directions

4. CONCLUSION

In this paper, a methodology for aggregating WPPs based on incoming wind direction under exact wind speeds was presented and assessed. Toward a realistic aggregated model that reflects the entire WPP response, an algorithm was employed to compute the actual exact wind speed experienced by every individual wind turbine within a WPP. Furthermore, the throughput of the aggregated models that are obtained depending on wind speed direction was studied and compared. The results showed the importance of the exact calculation of the speeds of the wind within the WPP in ensuring that the aggregated WPP model accurately represents real-world conditions. The results also highlighted the effect of the wind directions on the response of WPPs. It was concluded that the wind speed direction with 45° produces a larger WPP output power compared to that with other wind directions. The variability of wind speed direction over the year within a specific geographic area brings a substantial significance to the positioning of wind turbines within a WPP. A strategic positioning of the wind turbines is necessary to achieve maximum throughput from a WPP throughout the year under the prevailing wind speed direction.

The proposed wind direction based aggregation of WPPs as well as the exact wind speed calculations provide valuable insights for wind farm designers and grid operators into the dynamic behavior of large WPPs, the efficient benefiting of site characteristics, and the reduction of wind energy losses. By knowing the wind speed direction at the site and exact wind speed on every wind turbine within the farm, designers can more effectively assess the placement and performance of the turbines. The aggregated model of a WPP adequately reflects the output and dynamic response of the complete wind farm, which enables grid operators to enhance system planning and perform stability studies.

It is worth mentioning that the present work opens the door for further future research within the scope of WPP aggregation. For instance, practical relevance requires testing the proposed approach under multiple long-term wind speed regimes. This may represent a limitation of the current work. The presented simulation results in this work may also be compared with real-world implementation for benchmarking purposes. Additional work may also include comparing the proposed wind speed calculation algorithm with the probabilistic and statistical techniques of wind speed estimation. Also, artificial intelligence and machine learning methods such as clustering algorithms, deep hybrid models, and gated recurrent units can be employed to improve the wind speed estimations at the various locations within the WPPs to increase the accuracy of the aggregation models. All these research pathways provide opportunities to focus future efforts by researchers on developing robust and more realistic aggregation models of the WPPs.

FUNDING INFORMATION

Authors state no funding involved.

AUTHOR CONTRIBUTIONS STATEMENT

This journal uses the Contributor Roles Taxonomy (CRediT) to recognize individual author contributions, reduce authorship disputes, and facilitate collaboration.

Name of Author	C	M	So	Va	Fo	I	R	D	O	E	Vi	Su	P	Fu
Ali M. S. Al-Bayati	✓	✓	✓	✓	✓	✓	✓	✓	✓	✓	✓	✓	✓	
Huda Hamza Abdulkhudhur		✓	✓	✓	✓	✓	✓			✓	✓			

C : **C**onceptualization
M : **M**ethodology
So : **So**ftware
Va : **Va**lidation
Fo : **Fo**rmal Analysis
I : **I**nvestigation
R : **R**esources
D : **D**ata Curation
O : Writing - **O**riginal Draft
E : Writing - Review & **E**diting
Vi : **Vi**sualization
Su : **Su**pervision
P : **P**roject Administration
Fu : **Fu**nding Acquisition

CONFLICT OF INTEREST STATEMENT

Authors state no conflict of interest.

DATA AVAILABILITY

Data availability is not applicable to this paper as no new data were created or analyzed in this study.

REFERENCES

[1] American Clean Power Association, "Clean power quarterly market report Q3 2023." [Online] Available: https://cleanpower.org, 2023.

[2] H. Holttinen and B. H. Jørgensen, "IEA wind TCP annual report 2022." [Online] Available: https://iea-wind.org/wp-content/uploads/2023/10/IEA Wind TCP Annual Report 2022 Executive Summary. pdf, 2023.

[3] J. Lee and F. Zhao, "Global wind report 2022," 2022. [Online] Available: https://www.gwec.net/reports?t= 227262377152, Global Wind Energy Council, 2022.

[4] X. Jiao, D. Zhang, X. Wang, Y. Tian, W. Liu, and L. Xin, "Wind speed prediction based on error compensation," *Sensors*, vol. 23, no. 10, 2023, doi: 10.3390/s23104905.

[5] V. Romanuke, "Wind speed distribution direct approximation by accumulative statistics of measurements and root-mean-square deviation control," *Electrical, Control and Communication Engineering*, vol. 16, no. 2, pp. 65–71, 2020, doi: 10.2478/ecce-2020-0010.

[6] F. V. J. Silveira *et al.*, "Modelling wind speed with a univariate probability distribution depending on two baseline functions," *Hacettepe Journal of Mathematics and Statistics*, vol. 52, no. 3, pp. 808–827, 2023, doi: 10.15672/hujms.976348.

[7] M. Zhang, Y. Wang, H. Zhang, Z. Peng, and J. Tang, "A novel and robust wind speed prediction method based on spatial features of wind farm cluster," *Mathematics*, vol. 11, no. 3, 2023, doi: 10.3390/math11030499.

[8] A. B. Attya and T. Hartkopf, "Generation of high resolution wind speeds and wind speed arrays inside a wind farm based on real site data," in *Proceeding of the International Conference on Electrical Power Quality and Utilisation*, EPQU, 2011, pp. 164–169, doi: 10.1109/EPQU.2011.6128927.

[9] M. J. Mercado-Vargas, D. Gómez-Lorente, O. Rabaza, and E. Alameda-Hernandez, "Aggregated models of permanent magnet synchronous generators wind farms," *Renewable Energy*, vol. 83, pp. 1287–1298, 2015, doi: 10.1016/j.renene.2015.04.040.

[10] F. Xue, X. F. Song, K. Chang, T. C. Xu, F. Wu, and Y. Q. Jin, "Equivalent modeling of dfig based wind farm using equivalent maximum power curve," *IEEE Power and Energy Society General Meeting*, 2013, doi: 10.1109/PESMG.2013.6672848.

[11] A. M. S. Al-Bayati, F. Mancilla-David, and J. L. Domínguez-Garcíal, "Aggregated models of wind farms: current methods and future trends," in *NAPS 2016 - 48th North American Power Symposium, Proceedings*, 2016, doi: 10.1109/NAPS.2016.7747954.

[12] H. Sipeng, Z. Yangfei, L. Xianyun, and Y. Yue, "Equivalent wind speed model in wind farm dynamic analysis," in *2011 4th International Conference on Electric Utility Deregulation and Restructuring and Power Technologies (DRPT)*, IEEE, Jul. 2011, pp. 1751–1755, doi: 10.1109/DRPT.2011.5994181.

[13] H. Wang, C. Buchhagen, and J. Sun, "Methods to aggregate turbine and network impedance for wind farm resonance analysis," *IET Renewable Power Generation*, vol. 14, no. 8, pp. 1304–1311, 2020, doi: 10.1049/iet-rpg.2019.0339.

[14] L. Li, Y. M. Wang, and Y. Q. Liu, "Impact of wake effect on wind power prediction," in *IET Conference Publications*, 2013, doi: 10.1049/cp.2013.1827.

[15] L. Zhuonan and A. Xin, "Flatlands wind farm power generation and wake effect analysis based on jensen model," in *Asia-Pacific Power and Energy Engineering Conference, APPEEC*, 2013, doi: 10.1109/APPEEC.2013.6837159.

[16] W. Du, W. Dong, H. Wang, and J. Cao, "Dynamic aggregation of same wind turbine generators in parallel connection for studying oscillation stability of a wind farm," *IEEE Transactions on Power Systems*, vol. 34, no. 6, pp. 4694–4705, 2019, doi: 10.1109/TPWRS.2019.2920413.

[17] W. Dong, W. Du, X. Xie, and H. F. Wang, "An approximate aggregated impedance model of a grid-connected wind farm for the study of small-signal stability," *IEEE Transactions on Power Systems*, vol. 37, no. 5, pp. 3847–3861, 2022, doi: 10.1109/TPWRS.2021.3138107.

[18] X. Zhang and W. Wang, "Wind farm and wake effect modeling for simulation of a studied power system," *IEEE/PES Power Systems Conference and Exposition, PSCE* 2009, doi: 10.1109/PSCE.2009.4839929.
[19] M. T. Rahman, K. N. Hasan, and P. Sokolowski, "Evaluation of wind farm aggregation using probabilistic clustering algorithms for power system stability assessment," *Sustainable Energy, Grids and Networks*, vol. 30, 2022, doi: 10.1016/j.segan.2022.100678.
[20] A. Marinopoulos *et al.*, "Investigating the impact of wake effect on wind farm aggregation," in *IEEE PES Trondheim PowerTech: The Power of Technology for a Sustainable Society, POWERTECH*, 2011, doi: 10.1109/PTC.2011.6019323.
[21] N. Shabanikia, A. A. Nia, A. Tabesh, and S. A. Khajehoddin, "Weighted dynamic aggregation modeling of induction machine-based wind farms," *IEEE Transactions on Sustainable Energy*, vol. 12, no. 3, pp. 1604–1614, 2021, doi: 10.1109/TSTE.2021.3057854.
[22] J. Han, L. Li, H. Song, M. Liu, Z. Song, and Y. Qu, "An equivalent model of wind farm based on multivariate multi-scale entropy and multi-view clustering," *Energies*, vol. 15, no. 16, 2022, doi: 10.3390/en15166054.
[23] Y. Jin, D. Wu, P. Ju, C. Rehtanz, F. Wu, and X. Pan, "Modeling of wind speeds inside a wind farm with application to wind farm aggregate modeling considering LVRT characteristic," *IEEE Transactions on Energy Conversion*, vol. 35, no. 1, pp. 508–519, 2020, doi: 10.1109/TEC.2019.2938813.
[24] P. M. Anderson and A. Bose, "Stability simulation of wind turbine systems," *IEEE Power Engineering Review*, vol. PER-3, no. 12, pp. 32–32, 1983, doi: 10.1109/MPER.1983.5520133.
[25] Martínez and A. Medina, "A state space model for the dynamic operation representation of small-scale wind-photovoltaic hybrid systems," *Renewable Energy*, vol. 35, no. 6, pp. 1159–1168, 2010, doi: 10.1016/j.renene.2009.11.039.
[26] R. J. Barthelmie and L. E. Jensen, "Evaluation of wind farm efficiency and wind turbine wakes at the nysted offshore wind farm," *Wind Energy*, vol. 13, no. 6, pp. 573–586, 2010, doi: 10.1002/we.408.
[27] International Electrotechnical Commission, "IEC 61400-1 ed. 3: wind turbines – part 1: design requirements, amendment 1," 2009.
[28] S. T. Frandsen, "Turbulence and turbulence–generated structural loading in wind turbine clusters," 2007. [Online]. Available: https://backend.orbit.dtu.dk/ws/files/12674798/ris r 1188.pdf.
[29] E. Muljadi *et al.*, "Equivalencing the collector system of a large wind power plant," *IEEE Power Engineering Society General Meeting, PES*, 2006, doi: 10.1109/pes.2006.1708945.
[30] C. Jung and D. Schindler, "The role of the power law exponent in wind energy assessment: a global analysis," *International Journal of Energy Research*, vol. 45, no. 6, pp. 8484–8496, 2021, doi: 10.1002/er.6382.
[31] C. A. Lopez-Villalobos, O. Martínez-Alvarado, O. Rodriguez-Hernandez, and R. Romero-Centeno, "Analysis of the influence of the wind speed profile on wind power production," *Energy Reports*, vol. 8, pp. 8079–8092, 2022, doi: 10.1016/j.egyr.2022.06.046.

BIOGRAPHIES OF AUTHORS

Ali M. S. Al-Bayati received the B.S. and M.S. degrees in electrical engineering from the University of Baghdad, Baghdad, Iraq, in 2007 and 2010, respectively, and the Ph.D. degree in electrical engineering from University of Denver, Denver, CO, USA, in 2021. He is currently a faculty member at the College of Education Tuz Khurmatu, Tikrit University, Tuz Khurmatu, Salah Al-Din, Iraq. He was a faculty member at the Technical Engineering College-Kirkuk, Northern Technical University, Kirkuk, Iraq. His research interests include power systems modeling and optimization, renewable energy integration, and wide bandgap materials technology and its applications in power conversion systems. He can be contacted at email: ali.mah.salman@tu.edu.iq.

Huda Hamza Abdulkhudhur received the B.S. degree in electrical engineering from Tikrit University, Tikrit, Salah Al-Din, Iraq, and the M.S. degree in electrical engineering from Razi University, Kermanshah, Iran, in 2018. Since 2019, she has been a faculty member at the Technical Engineering College-Kirkuk, Northern Technical University, Kirkuk, Iraq. In August 2025, she transitioned to the Technical Engineering College for Computer and AI-Kirkuk within the same university, where she currently serves as an assistant lecturer in the Department of Cybersecurity Techniques Engineering. Her research interests include smart grid systems, integration of renewable energy into power systems, and optimization of electrical system performance, with a particular focus on leveraging fiber-optic communication and internet of things technologies to support the realization of intelligent, adaptive, and sustainable electrical infrastructures. She can be contacted at email: hudahamza.abdulkhudhur@ntu.edu.iq.